Atmospheric Environment 127 (2016) 293–302

Contents lists available at ScienceDirect

Atmospheric Environment

journal homepage: www.elsevier.com/locate/atmosenv

Airborne measurements and emission estimates of greenhouse gases and other trace constituents from the 2013 California Yosemite Rim wildfire

E.L. Yates [a, *], L.T. Iraci [a], H.B. Singh [a], T. Tanaka [a], M.C. Roby [a, b], P. Hamill [b], C.B. Clements [b], N. Lareau [b], J. Contezac [b], D.R. Blake [c], I.J. Simpson [c], A. Wisthaler [d, e], T. Mikoviny [e], G.S. Diskin [f], A.J. Beyersdorf [f], Y. Choi [f, g], T.B. Ryerson [h], J.L. Jimenez [i], P. Campuzano-Jost [i], M. Loewenstein [a], W. Gore [a]

[a] NASA Ames Research Center, Moffett Field, CA, USA
[b] San José State University, San José, CA, USA
[c] UC Irvine, Irvine, CA, USA
[d] Institute of Ion Physics and Applied Physics, University of Innsbruck, Austria
[e] Department of Chemistry, University of Oslo, Norway
[f] NASA Langley, Hampton, VA, USA
[g] Science Systems and Applications, Inc., Hampton, VA 23666, USA
[h] NOAA ESRL Boulder, CO, USA
[i] University of Colorado, Boulder, CO, USA

HIGHLIGHTS

- Airborne measurements of trace gases downwind of an exceptionally large wildfire.
- Measurements during the Rim wildfire intense and smoldering burning phases.
- Assessment of emission ratios, emission factors and combustion efficiency.
- Dataset to support forestry and regional air quality management.

ARTICLE INFO

Article history:
Received 19 April 2015
Received in revised form
6 December 2015
Accepted 17 December 2015
Available online 19 December 2015

Keywords:
Wildfire
Trace gases
Emission factors
Enhancement ratios
Western US

ABSTRACT

This paper presents airborne measurements of multiple atmospheric trace constituents including greenhouse gases (such as CO_2, CH_4, O_3) and biomass burning tracers (such as CO, CH_3CN) downwind of an exceptionally large wildfire. In summer 2013, the Rim wildfire, ignited just west of the Yosemite National Park, California, and burned over 250,000 acres of the forest during the 2-month period (17 August to 24 October) before it was extinguished. The Rim wildfire plume was intercepted by flights carried out by the NASA Ames Alpha Jet Atmospheric eXperiment (AJAX) on 29 August and the NASA DC-8, as part of SEAC^{4}RS (Studies of Emissions, Atmospheric Composition, Clouds and Climate Coupling by Regional Surveys), on 26 and 27 August during its intense, primary burning period. AJAX revisited the wildfire on 10 September when the conditions were increasingly smoldering, with slower growth. The more extensive payload of the DC-8 helped to bridge key measurements that were not available as part of AJAX (e. g. CO). Data analyses are presented in terms of emission ratios (ER), emission factors (EF) and combustion efficiency and are compared with previous wildfire studies. ERs were 8.0 ppb CH_4 (ppm CO_2)$^{-1}$ on 26 August, 6.5 ppb CH_4 (ppm CO_2)$^{-1}$ on 29 August and 18.3 ppb CH_4 (ppm CO_2)$^{-1}$ on 10 September 2013. The increase in CH_4 ER from 6.5 to 8.0 ppb CH_4 (ppm CO_2)$^{-1}$ during the primary burning period to 18.3 ppb CH_4 (ppm CO_2)$^{-1}$ during the fire's slower growth period likely indicates enhanced CH_4 emissions from increased smoldering combustion relative to flaming combustion. Given the magnitude of the Rim wildfire, the impacts it had on regional air quality and the limited sampling of wildfire emissions in the western United States to date, this study provides a valuable dataset to support forestry

* Corresponding author.
E-mail address: emma.l.yates@nasa.gov (E.L. Yates).

http://dx.doi.org/10.1016/j.atmosenv.2015.12.038

and regional air quality management, including observations of ERs of a wide number of species from the Rim wildfire.

1. Introduction

Emissions from biomass burning (defined here as the open burning of biomass, including wildfires, prescribed fires and agricultural fires) are an important source of a wide range of trace gases and particles that can impact local, regional and global air quality, climate forcing, biogeochemical cycles and human health (Crutzen and Andreae, 1990; Bein et al., 2008; Pfister et al., 2008; Aurell and Gullett, 2013). Biomass burning emissions are one of the primary causes for the annual variability in growth rates of several trace gases, including carbon dioxide (CO_2) and methane (CH_4) (Langenfelds et al., 2002; Simpson et al., 2006). Because of the importance of these emissions and the projected increases in wildfire activity in many regions due to climate change and fuel management strategies (Fried et al., 2004; Westerling et al., 2006; Yue et al., 2013; Hurteau et al., 2014), measurements of emissions from wildfires are crucial to a better understanding of how biomass burning influences and interacts with the Earth system.

United States (US) temperate biomass burning carbon emissions are relatively small (about 0.5%) compared to total global emissions (van der Werf et al., 2010). However, such burns have the potential to significantly impact local and regional air quality (Sapkota et al., 2005; Singh et al., 2012). Long range transport of biomass burning emissions can cause air quality standards to be exceeded hundreds and thousands of kilometers downwind of the fire source (Jaffe et al., 2013; Wigder et al., 2013; Real et al., 2007; Sapkota et al., 2005).

In the US, wildland fires can be divided into two categories: prescribed fires and wildfires (Urbanski, 2013). Prescribed fires are ignited by land management programs to reduce wildfire hazards, improve wildlife habitats and increase access (Dale, 2006). The majority of prescribed burns in the western US occur outside of the wildfire season (June–September) (Urbanski, 2013). In the western US, wildfires dominate over prescribed fires, accounting for 85% of the burned area between 2002 and 2010 (NIFC, 2015). The majority of wildfires occur when the "Fire Danger" is at high levels and when forest floor moisture is at a minimum (Deeming et al., 1978). Western wildfires typically occur under conditions that result in the consumption of fuels (large dead woody debris, duff, and tree canopy) that are not normally burned in prescribed fires. This could result in different emissions from wildfires compared to prescribed fires as noted by Urbanski (2013).

The extent to which wildfires contribute to atmospheric trace gas budgets is uncertain and varies intra- and inter-seasonally due to the unique and episodic nature of wildfires. Measured trace gas concentrations vary due to degree of dilution and mixing with other air mases, fuel type and condition, meteorological conditions, the fire combustion processes and location and distance from the fire where the data are collected due to chemistry and aging (Jaffe et al., 2013; Trentmann et al., 2003; Reid et al., 2005; Real et al., 2007; Yokelson et al., 2013).

Typically wildfire emissions are expressed as enhancement ratios (ERs) or emission factors (EFs) and modified combustion efficiency ($MCE = \Delta CO_2/(\Delta CO_2 + \Delta CO)$). ERs are estimated by first calculating the excess mixing ratio of a trace gas, X, compared to its average background value ($\Delta X = X_{plume} - X_{bkgd}$). Fig. 1 shows background mixing ratios for a large number of trace constituents measured over the U. S. by the NASA DC-8. Background mixing ratios are determined by using a CO filter (lowest quartile) that removed most pollution influences. ΔX is then divided by the excess mixing ratio of a reference gas (RG), typically carbon monoxide (CO) or CO_2 (Andreae and Merlet, 2001), see Equation (1). The ER is the slope of ΔX/ΔRG, while forcing the intercept through zero (since the background concentration is typically well known and variability in the plume can affect the intercept if it is not forced) (Yokelson et al., 1999; Akagi et al., 2012). The emission factor, EF, quantifies the amount of trace gas, X, emitted per kilogram of biomass burned and can be calculated using the carbon mass balance technique described by Yokelson et al. (1999). MCE characterizes the relative amounts of flaming and smoldering combustion within a fire. MCE ranges from 0.65 to 0.99, but is typically near 0.80 for smoldering, while pure flaming combustion has an MCE of 0.99. An overall MCE of 0.90 suggests roughly equal flaming and smoldering combustion (Akagi et al., 2011).

$$ER = \left(X_{plume} - X_{bkgd}\right) \Big/ \left(RG_{plume} - RG_{bkgd}\right) \quad (1)$$

ERs, EFs and MCE are essential parameters for atmospheric chemical transport models used to understand and predict the impacts of wildfire emissions. However, in the western US, emission estimates rely largely on measurements from prescribed fires, which may not be a suitable proxy for wildfire emissions. There is currently limited information on emissions from wildfires occurring in the western US during the wildfire season (Urbanski, 2013).

This paper presents airborne in situ measurements of greenhouse gases (CO_2, CH_4 and ozone (O_3)), biomass burning tracers (CO and acetonitrile (CH_3CN)), and other constituents downwind of the exceptionally large Rim wildfire. The Rim wildfire started from an illegal campfire that burned out of control on 17 August 2013, about 13 km east of Groveland, California. Over the next several weeks and months it moved eastward burning a total of 257,134 acres of brush, oaks, and pine conifer stands in steep, rugged terrain

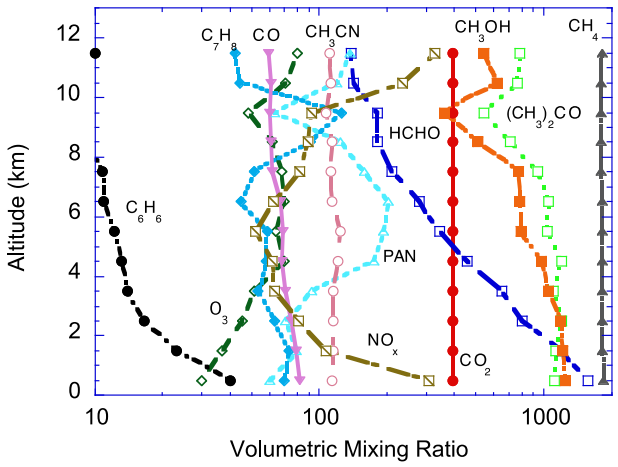

Fig. 1. Measured mean U.S. background mixing ratios of selected trace gases as measured by the DC-8 during SEAC^{4}RS. Background mixing ratios correspond to the lowest quartile of CO. Mixing ratios are in units of ppm for CO_2, ppb for CH_4, CO and O_3, and ppt for all other species.

(elevation ranges from < 500 to > 2000 m above sea level (m.a.s.l)) within the Stanislaus National Forest and into Yosemite National Park (37.86° N, 120.09° W). Airborne data from four flights that sampled emissions from the Rim wildfire are discussed. Three flights sampled downwind of the Rim wildfire during its intense, primary burning period; one by the Alpha Jet Atmospheric eXperiment (AJAX) on 29 August, and two by the NASA DC-8, as part of the Studies of Emissions and Atmospheric Composition, Clouds, and Climate Coupling by Regional Surveys (SEAC^{4}RS) mission, which sampled mixed smoke from a number of fires throughout the Western US on 26 and 27 August. Another AJAX flight on 10 September sampled emissions from the fire during its increased smoldering, slower growth period.

2. Experimental approach

The two AJAX flights measured in situ CO_2, CH_4 and O_3 mixing ratios. CO_2 and CH_4 were measured using cavity ring-down spectroscopy (Picarro, Inc., model 2301-m), an instrument widely described in the literature (Chen et al., 2010; Tanaka et al., 2012; Karion et al., 2013; Tadić et al., 2014). Raw data was processed by multiplying by the calibration factors, determined from NOAA whole air standards, traceable to the WMO scale, and by application of the water vapor corrections provided by Chen et al. (2010) to calculate the dry mixing ratios of CO_2 and CH_4. Data were also filtered to remove spikes in the data as a result of varying instrument cell cavity pressure and data were averaged and reported at 3 s intervals. The overall uncertainty is determined to be 0.14 ppm for CO_2 and 2.8 ppb for CH_4. O_3 is measured by ultraviolet (UV) absorption (2B Technologies Inc., model 205). Raw data is multiplied by the calibration factors, determined from an O_3 calibration source (2B Technologies, model 306) referenced to the NIST scale. Data is averaged and reported at 10 s intervals with an overall uncertainty of the airborne O_3 measurements estimated at 3.0 ppbv.

SEAC^{4}RS was a NASA led airborne mission during summer of 2013 over the continental US (https://espo.nasa.gov/missions/seac4rs). Among its many objectives was to investigate the influence of biomass burning emissions, and their interactions with urban pollution, on regional air quality and climate. The main airborne platform for this objective was the NASA DC-8 aircraft equipped with 28 in-situ and remote sensing instruments to measure greenhouse gases, O_3 precursors and oxidation products, reactive nitrogen, and aerosol composition and physical/optical properties, and several unique tracers of pollution with high sensitivity. Toon et al. (2015) present details of the SEAC^{4}RS mission, including instrumentation, in an overview paper. The same platform, similarly equipped (Jacob et al., 2010) has been previously used to investigate fire emissions resulting from Boreal fires during ARCTAS (e.g. Singh et al., 2010; Simpson et al., 2011; Hecobian et al., 2011). The DC-8 observations complement those measured from AJAX by filling gaps with additional trace gas species that could not be measured by AJAX. Although the DC-8 sampled many wildfires and agricultural fires, here we will limit our study to the Rim wildfire investigations on 26 and 27 August 2013. The complete data sets are available at http://www-air.larc.nasa.gov/cgi-bin/ArcView/seac4rs?MERGE=1. Additional studies of the Rim Fire during the SEAC^{4}RS flights are presented by Peterson et al. (2014), Saide et al. (2015) and Forrister et al. (2015). The following references provide further information on SEAC^{4}RS measurements of CO (Sachse et al., 1987), CH_4, C_6H_6, C_7H_8 (Simpson et al., 2011), CO_2 (Vay et al., 2003) CH_3CN, CH_3OH, CH_3COCH_3 (Wisthaler et al., 2002), O_3, NOx (Weinheimer et al., 1994), PAN (Huey, 2007), NO_3 (Dibb et al., 2003), BC (Moteki and Kondo, 2007), SO_4 and OA (DeCarlo et al., 2008).

SEAC^{4}RS flight data were filtered to focus primarily on emissions from the Rim wildfire. Firstly data was segregated by geographical location (37.8–44° N, 102–120° W, altitude <8 km) and secondly filtered based on ΔCH_3CN values ($\Delta CH_3CN > 0.2$ ppb). Given that ΔCH_3CN is a preferred tracer of biomass burning as its relative enhancement ($\Delta CH_3CN/\Delta CO$) is nearly independent of combustion efficiency (Singh et al., 2012; Hornbrook et al., 2011), this filter, combined with the geographic filter, selects the data from primarily the Rim wildfire smoke plume. The section of the SEAC^{4}RS flight tracks used in this analysis is shown in Fig. 7.

3. Results

Within the first few weeks after the Rim fire ignited, fire activity was generally high to extreme (National Fire and Aviation Management Web Applications, FAMWEB, 2014). After 8 September 2013, fire progression remained below 1500 acres per day as the fire was gradually contained (Inciweb, 2013), with 100% containment achieved on 24 October 2013. Fig. 2 shows the progression and activity of the Rim Fire and timing of the airborne measurement flights.

3.1. Intense burning (26–29 August 2013)

Three flights measured emissions from the Rim wildfire during its intense, primary burning period. The first two flights were on 26 and 27 August 2013 by the NASA DC-8 aircraft followed by an AJAX flight on 29 August 2013. During all three flights, the main smoke plume from the Rim wildfire was transported by southwesterly winds impacting regions to the north and northeast including Lake Tahoe, northern Sierra Nevada mountain communities, and northern Nevada. Some smoke detrained at lower altitudes and settled into near-by valleys, as shown in Fig. 3. Air quality maps reported highly elevated values of particulate matter (PM 2.5) to the north and northeast of the fire (Airnow, 2015), see Fig. S1.

The extent and progression of the smoke plume was analyzed using the California State University Mobile Atmospheric Profiling System (CSU-MAPS) (Clements and Oliphant, 2014). The mobile profiling system is mounted on a truck and includes a scanning Doppler Lidar (Halo Photonics, Ltd., Streamline 75) and radiosonde system (GRAW Radiosondes GmbH & Co. KG, model GS-E). On 29 August 2013, the CSU-MAPS was operated from Donnell Vista (38.342° N, 119.925° W, elevation 1921 m a.s.l), just north of the main fire exclusion zone and within 0.5 km of the AJAX flight path.

The Lidar provided information on the dynamics and progression of the Rim wildfire plume. Three distinct layers were observed in the attenuated backscatter coefficient and vertical velocities (shown in Fig. 4). The local convective boundary layer extended from the surface to 3000 m a.s.l (also evident in radiosonde data, see Fig. S2) and was rich in smoke from the Rim wildfire. The 3000–4000 m a.s.l layer was also rich in smoke, likely representing smoke injected to greater heights caused by overshooting of the fire plume beyond the depth of the convective boundary layer. Above 4000 m a.s.l the dry, free-troposphere is devoid of backscatter.

The flights targeting the Rim wildfire plume on 26, 27 and 29 August 2013 all took place in the afternoon, at a time when the concentrated plume within the boundary layer was starting to dissipate. During the time of the AJAX flight the boundary layer smoke plume was less dense than an hour prior, and smoke is at all levels below 4000 m a.s.l (see vertical line in Fig. 4 for timing of the AJAX flight).

For each flight, trace gas enhancements (e.g. ΔCO_2, ΔCH_4, ΔO_3) were calculated based on subtracting the average background value for each species from the measured mixing ratios (e.g. $\Delta X = X - X_{bkgd}$). For AJAX data the background is defined as an

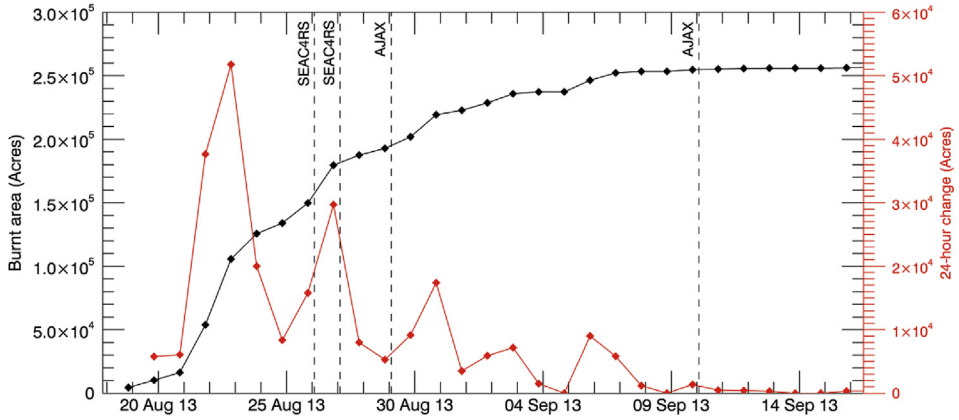

Fig. 2. Time series of total acres burned and 24-h change in acres burned based from daily fire reports (adapted from http://inciweb.nwcg.gov/incident/3660/). Timings of the AJAX and SEAC^{4}RS flights are shown as dashed lines.

Fig. 3. Photograph of the main smoke plume and low altitude smoke plume (valley haze) in Bear Valley (38.367° N, 120.170° W) taken in-flight on 29 August 2013.

upwind section of the flight. For example, on 29 August 2013 background is calculated from the average mixing ratios observed in transects above the smoke plume; see Fig. 5 (background average CO_2: 393.48 ± 0.38 ppm, CH_4: 1845 ± 5 ppb, O_3: 49 ± 8 ppb). To estimate sensitivity associated with determining background mixing ratios, the time period used to calculate the background was altered resulting in negligible effects (within the 1σ deviation), providing realistic time periods are used. For SEAC^{4}RS data the background was calculated from the average backgrounds shown in Fig. 1.

Large deviations from background values were observed in-flight for many trace gas species. For example, notable values of ΔCO_2, ΔCH_4 and ΔO_3 during the 29 August 2013 AJAX flight occur in four instances (see Fig. 5): Within the San Joaquin Valley (SJV) boundary layer (<2000 m a.s.l. at 21:30 UTC, located upwind of the wildfire), the main smoke plume encounter (22:16 UTC, 4400 m a.s.l.), sampling above the foothills upwind of the wildfire (22:25 UTC, 3100 m a.s.l.) and sampling the smoke-filled valley haze (22:37 UTC, 2100–3700 m a.s.l.). ΔCO_2 in the SJV boundary layer is depleted compared background, consistent with uptake by the biosphere. In contrast, ΔCH_4 within the SJV boundary layer is enhanced due to local, surface-based sources in the region. Above

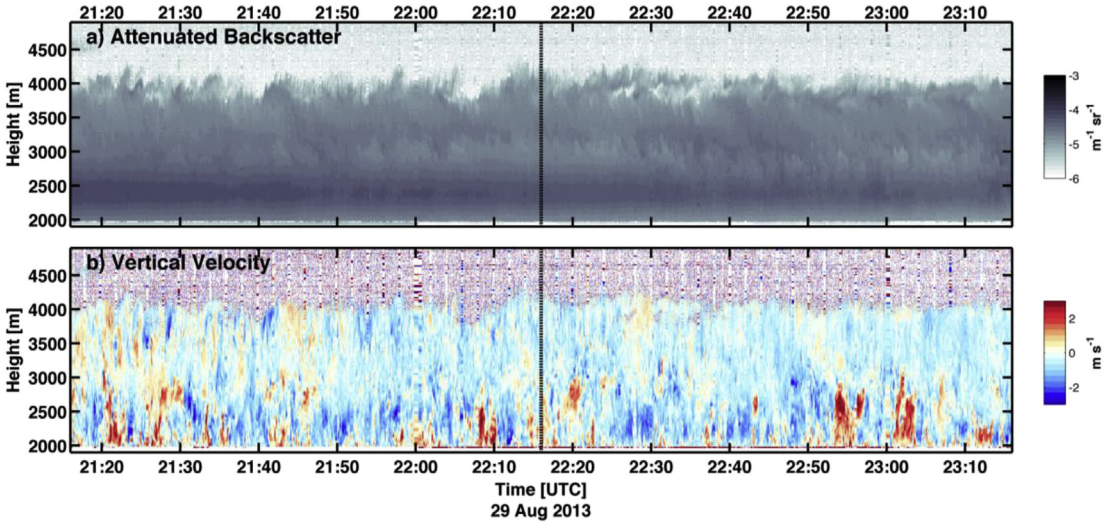

Fig. 4. Lidar profiles of a) attenuated backscatter coefficient (m^{-1} sr^{-1}) and b) vertical velocity (m s^{-1}) taken at Donnell Vista, CA (38.342° N, 119.925° W) on 29 August 2013. The black vertical line represents the time that the AJAX flight sampled the main smoke plume from the Rim wildfire (Local time = UTC − 7 h). Height is meters above sea level (m a.s.l) (For interpretation of the references to colour in this figure legend, the reader is referred to the web version of this article.).

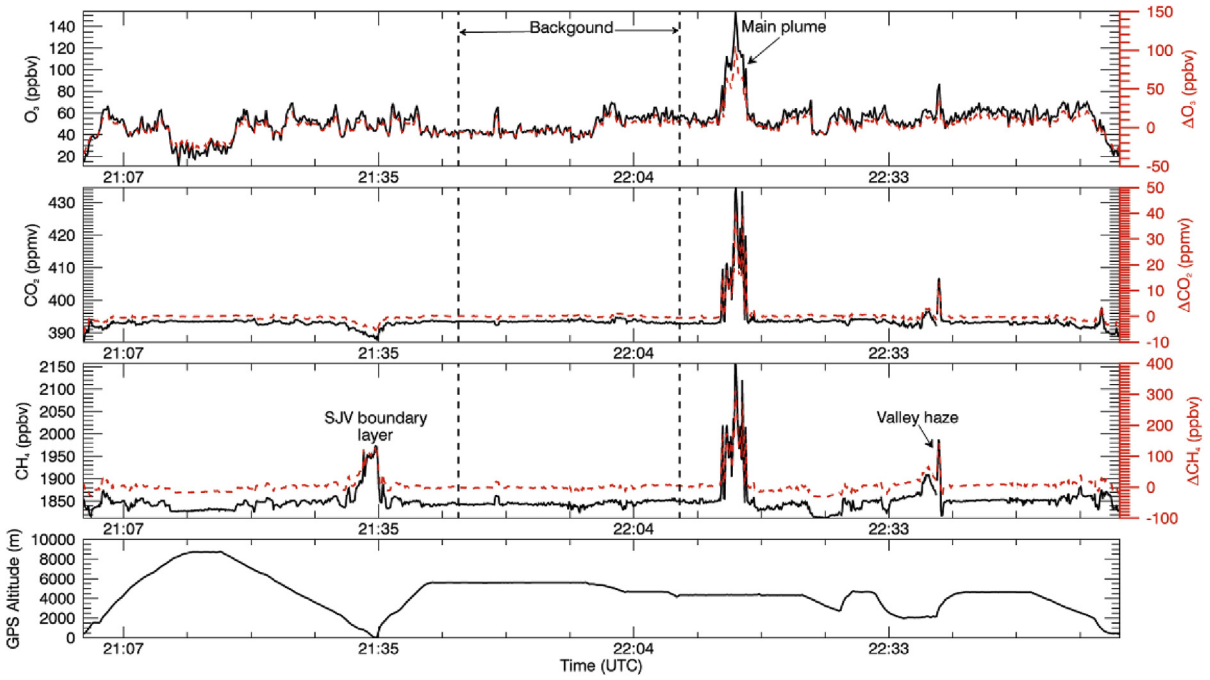

Fig. 5. Time series plots of CO_2, CH_4, O_3 and altitude from the AJAX flight on 29 August 2013 (Local time = UTC − 7 h). Trace gas enhancements from background values (ΔCO_2, ΔCH_4, ΔO_3) are plotted as red dashed lines. Black dashed lines represent the region used to define background trace gas values (For interpretation of the references to colour in this figure legend, the reader is referred to the web version of this article.).

the Sierra Nevada foothills upwind (southwest) of the fire ΔCO_2 is slightly depleted and ΔCH_4 significantly depleted, consistent with biospheric uptake and limited local CH_4 emissions in this region. Large enhancements were observed when sampling the main smoke plume (maximum ΔCO_2: 41.14 ppm, maximum ΔCH_4: 312 ppb, maximum ΔO_3: 105 ppb, mean altitude: 4.4 km a.s.l) and within the smoke-filled valley haze (maximum ΔCO_2: 13.29 ppm, maximum ΔCH_4: 140 ppb, maximum ΔO_3: 38 ppb, mean altitude: 2.4 km a.s.l).

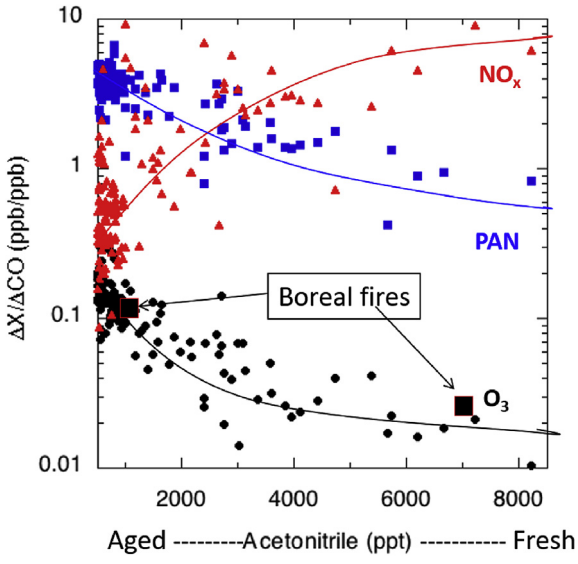

Fig. 6. Evolution of key constituents in the Rim wildfire plume during 0–2 day transport time measured by SEAC[4]RS. Y-axis represents the ratio of ΔNOx/ΔCO (red), ΔPAN/ΔCO (blue) and $\Delta O_3/\Delta CO$ (black) and X-axis shows mixing ratio of CH_3CN (a fire tracer) as an indicator of air mass age from wildfire emissions measured during SEAC[4]RS (Diskin et al., 2002; Huey, 2007; Weinheimer et al., 1994) (For interpretation of the references to colour in this figure legend, the reader is referred to the web version of this article.).

While sampling the Rim wildfire smoke plume, AJAX is limited to sampling only the top of the plume (~4.4 km), as the aircraft cannot descend to deep within the plume. When AJAX overflew the Lidar (which observed smoke to 4 km a.s.l), AJAX reported CO_2, CH_4 and O_3 mixing ratios at 4.4 km a.s.l close to background values, consistent with the Lidar observations that the smoke was not impacting higher altitudes over the measurement site. The main Rim wildfire plume captured by AJAX was located ~6 km to the SE from the Lidar site at 4.4 km. Variation in plume height between the two sites is likely given the complex local topography and the changing plume dynamics. The Lidar data confirms that when AJAX samples the top of the smoke plume it is sampling smoke which has overshot the boundary layer and is not sampling the boundary layer itself.

AJAX observed large enhancements in ΔO_3 at the top of the Rim wildfire plume on 29 August 2013 (maximum ΔO_3: 105 ppb). Enhanced O_3 was not reported at near-by surface sites (e.g. Yosemite national park (Turtleback Dome, CA) and Reno/Sparks (NV)), even though these surface sites were impacted by the wildfire plume, indicated by high PM2.5 levels (see Fig. S1). ΔO_3 observations from a nearby valley (valley haze, Fig. 5) confirm less ΔO_3 within the valley boundary layer (and further from the main fire activity (maximum ΔO_3: 38 ppb)). Previous studies of O_3 formation within wildfire plumes show varying rates of production, from O_3 depletion to substantial amounts (e.g. Bein et al., 2008; Pfister et al., 2008; Jaffe and Wigder, 2012; Singh et al., 2012). In this case, AJAX data shows significant O_3 formation within the upper layers of the Rim wildfire smoke plume.

The estimated age of the smoke plume (time since emission) can be calculated by dividing the distance of the smoke downwind of the fire by the average wind speed at the altitude the smoke is sampled; see Equation (2) (Akagi et al., 2013). We estimate the AJAX measurements of the main plume were ~1.2 h downwind of the

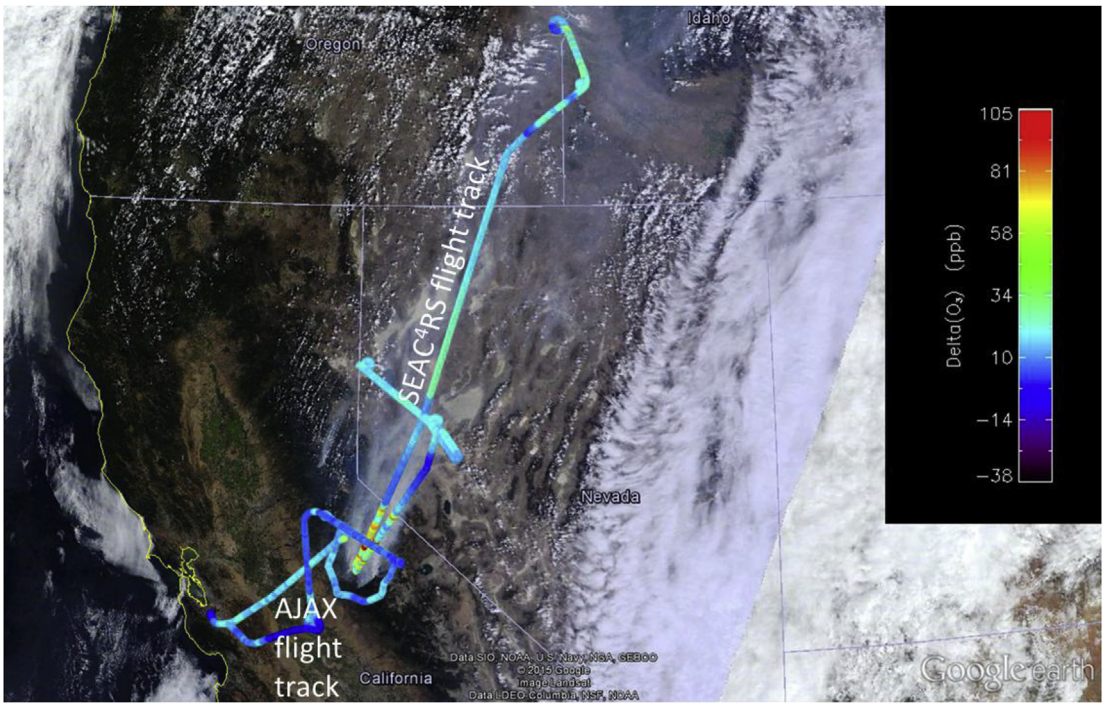

Fig. 7. Flight paths of: SEAC^{4}RS 26/27 August 2013 (37.8–44° N, 102–120° W, altitude <8 km) and AJAX 29 August 2013, data points are colored by ΔO_3 (deltaO_3). Co-plotted with MODIS Terra satellite image from 26 August 2013 in Google™ Earth.

Rim wildfire (~50 km from the center of the Rim wildfire, average wind speed at 4 km a.s.l was 11.8 m/s). Previous work has reported an immediate decrease in O_3 at the source of the fire due to rapid reaction of background O_3 with high levels of NO within the fire plume (Evans et al., 1974; Akagi et al., 2013). O_3 levels can rebound within the plume rapidly, as little as 0.5 h after downwind (Akagi et al., 2013), with a peak in O_3 being reached within ~1 h (Packham and Vines, 1978). AJAX O_3 measurements occur within the window of rapid O_3 formation and support evidence presented in prior work.

$$\textit{Time since emission} = \textit{sample distance from source } (m) \Big/ \textit{average wind speed } \left(\frac{m}{s}\right) \quad (2)$$

Comparing the main plume of the Rim wildfire with the smoke-filled valley haze highlights the markedly different conditions at each location. The main smoke plume overshot the top of the boundary layer and at 4.4 km a.s.l encountered an average wind speed of 14.7 m/s and direction of ~197°, whereas low-altitude smoke, at 2.1 km a.s.l within the boundary layer at Bear Valley (38.367° N, 120.170° W) encounters an the average wind speed of 5.2 m/s and direction of ~239°. The main plume and valley haze also differ in their compositions; for example ER's were 2.0 ppb O_3 (ppm CO_2)$^{-1}$ and 6.7 ppb CH_4 (ppm CO_2)$^{-1}$ within the main smoke plume, compared to 2.7 ppb O_3 (ppm CO_2)$^{-1}$ and 8.7 ppb CH_4 (ppm CO_2)$^{-1}$ within the valley haze. Although ER's for ΔO_3 and ΔCH_4 (relative to ΔCO_2) are higher within the valley, the overall, absolute values of ΔO_3, ΔCH_4 and ΔCO_2 are less within the valley haze compared to the main plume. Differences in smoke constituents within the two locations may be because smoke sampled within the valley is within the boundary layer. Lidar observations indicate that the boundary layer contains a more concentrated plume than what overshoots the top of the boundary layer and is sampled as the main plume by the AJAX flight (see Fig. 4). Smoke within the valley may also be more aged with respect to the main plume as wind speeds within the valley are reduced compared to aloft, meaning dispersion will be slower, or the valley haze may be more representative of more smoldering combustion (with minimal plume rise) as opposed to more flaming combustion (and convective plume).

The two SEAC^{4}RS flights provide additional context to AJAX data by measuring multiple tracers of biomass burning emissions (e.g. CO, CH_3CN) and chemically reactive species involved in O_3 formation including both PAN (peroxyacetyl nitrate) and NOx (NO and NO_2). Fig. 6 shows the complex relationships between ΔCH_3CN and the ERs (relative to ΔCO) of key species involved in O_3 formation. Fresh wildfire plumes (indicated by higher ΔCH_3CN mixing ratios) contain negligible enhancements of ΔO_3 and ΔPAN and higher levels of ΔNO_x. As plumes age the moderate-high levels of ΔNO_x are depleted in association with O_3 and PAN formation. The average ERs observed by SEAC^{4}RS are 0.01 for $\Delta O_3/\Delta CO$ (ppb/ppb), 2.6 for $\Delta PAN/\Delta CO$ (ppt/ppb) and 3.8 for $\Delta NOx/\Delta CO$ (ppt/ppb), and are similar to values reported by Singh et al. (2012). The enhancements represent some aging of the plume from the fit-curves shown in Fig. 6.

Previous studies have reported that O_3 production within wildfire plumes can occur over a range of time intervals, with O_3

production being more rapid in warmer environments, for example Hobbs et al. (2003) observed ΔO_3 of 98 ppb in less than 30 min of aging in South African biomass burning plumes. SEAC^{4}RS flights sampled fresh Rim wildfire emissions on 26 August 2013 and aged emissions on 27 August 2013. SEAC^{4}RS observed elevated ΔO_3 close to the source (maximum ΔO_3 of 100 ppb) which remained elevated (ΔO_3 > 40 ppb) to ~100 km downwind (estimated age: 3.6 h, average altitude ~4 km a.s.l, average wind speed: 7.6 m/s); see Fig. 7. AJAX and SEAC^{4}RS flights observed similar O_3 emissions from the Rim wildfire on different days during the intense, primary burning period, with both flights supporting the concept of rapid O_3 formation within the Rim wildfire plume.

3.2. Increased smoldering (10 September 2013)

During the second AJAX flight on 10 September 2013 the Rim wildfire was 80% contained and had burned 250,000 acres. The previous night, easterly downslope winds brought smoke from the Rim wildfire to the San Joaquin Valley (SJV). A morning inversion over SJV kept smoke impacts high for the region. Air quality maps report elevated PM 2.5 in a large dispersed area surrounding the fire (Airnow, 2015), see Fig. S3. As the day progressed, vertical mixing within the convective boundary layer improved air quality.

The second AJAX flight took place between 14:00–16:00 local time (21:00–23:00 UTC). The aircraft flew a descending profile over Castle airport, in the SJV, then proceeded to twice circumnavigate the Rim wildfire, sampling an outer and an inner circle. Sharp increases in ΔCO_2 and ΔCH_4 were observed within the SJV boundary layer and within the Rim wildfire smoke encounters, as seen in Fig. 8 (O_3 data collection was unsuccessful for this flight).

On 10 September 2013, ΔCH_4 and ΔCO_2 were enhanced within the SJV boundary layer. Smoke from the Rim wildfire influenced the boundary layer and outweighed the effects of biosphere uptake, resulting in increasing ΔCO_2 (in contrast to 29 August 2013). ΔCO_2 values within the SJV boundary layer were a similar order of magnitude to those observed within the smoke plume (see Fig. 8).

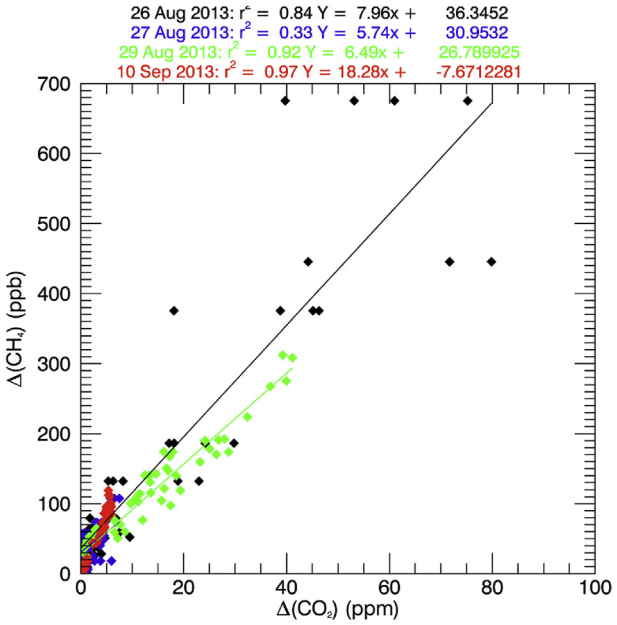

Fig. 9. Relationship between CH_4 and CO_2 enhancements from the Rim wildfire plume measured during flights on 26 August (black) and 27 August (blue, aged smoke), 29 August (green) and 10 September (red) 2013 (For interpretation of the references to colour in this figure legend, the reader is referred to the web version of this article.).

The maximum ΔCO_2 within the SJV boundary layer (<1 km a.s.l) is 8.36 ppm, compared to maximum ΔCO_2 within the outer circle smoke encounter of 5.90 ppm, and 9.91 ppm within the inner circle. Maximum ΔCH_4 values for the entire flight were observed within the SJV boundary layer, suggesting that local, surface-based sources were present in addition to the Rim wildfire emissions. Maximum ΔCH_4 within the SJV boundary layer is 334 ppb; within the outer circle smoke encounter it is 119 ppb and 159 ppb within the inner circle smoke plume encounter.

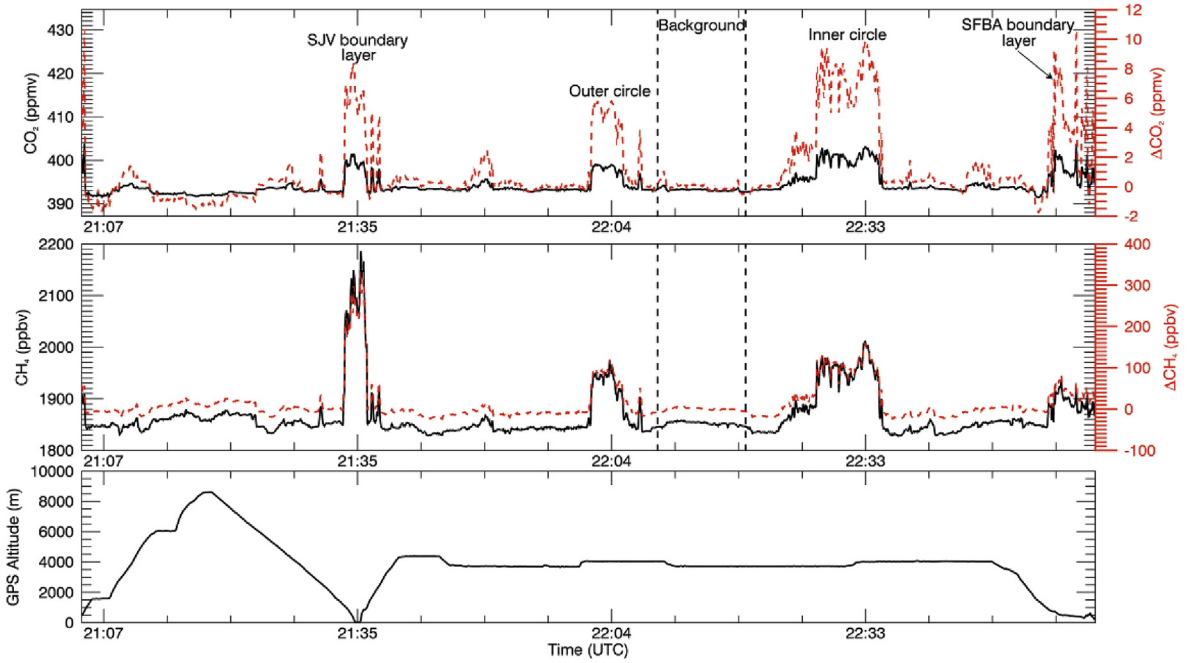

Fig. 8. Time series of CO_2 (top), CH_4 (middle) and altitude (bottom) from AJAX flight on 10 September 2013 (local time = UTC − 7 h). Trace gas enhancements from background values (ΔCO_2, ΔCH_4) are plotted as red dashed lines. Black dashed lines indicate the region used to define background trace gas values (For interpretation of the references to colour in this figure legend, the reader is referred to the web version of this article.).

3.3. Emission measurements

The ER for ΔCH_4 relative to ΔCO_2 is used to compare all four flights (Fig. 9). The SEAC^{4}RS data has been separated by day of flight. The 26 August 2013 SEAC^{4}RS flight and both AJAX flights show strong correlations within the Rim wildfire smoke plumes ($R^2 = 0.84–0.97$), as all three flights flew within close vicinity of the Rim wildfire, sampling very fresh emissions (within a few hours). The SEAC^{4}RS flight on 27 August is less well correlated ($r^2 = 0.33$); this flight sampled aged smoke from the Rim wildfire (up to ~2.3 days old). Dilution as the smoke plume ages as well as the presence of other wildfires impact the emission ratios within aged plumes, reducing the $\Delta CH_4/\Delta CO_2$ correlation. Calculated fresh plume CH_4 ER's were 6.5–8.0 ppb CH_4 (ppm CO_2)$^{-1}$ during the intense, primary burning period (flights on 26 and 29 August 2013). The good agreement between CH_4 ER's during the period between 26 and 29 August 2013 is likely due to a similarity in fire conditions and fuels burned on these days, as well as the proximity of the flights to the emission source. During the increased smoldering period of the Rim wildfire (AJAX flight on 10 September 2013), the CH_4 ER increased to an average of 18.3 ppb CH_4 (ppm CO_2)$^{-1}$, in close proximity to the emission source. CH_4 ER in the aged smoke was slightly less compared to the fresh plume at 5.7 ppb CH_4 (ppm CO_2)$^{-1}$ on 27 August 2013.

The change in CH_4 ER within the fresh plume from 6.5 to 8.0 ppb CH_4 (ppm CO_2)$^{-1}$ to 18.3 ppb CH_4 (ppm CO_2)$^{-1}$ implies a change in fire conditions, indicating an increase in smoldering combustion relative to flaming combustion and changes in fuel/materials involved. During the more active fire stages (prior to 5 September 2013) the major fuels involved were categorized by the United States Department of Agriculture (USDA) as fuel model 5 (brush (2 feet)) consisting of brush, oaks and pines, in the later stage of the fire. On 10 September 2013, the major fuels involved were categorized by USDA fuel model 9 (hardwood litter) consisting of pine, fir, conifer stands mixed with patches of brush and open grasses (FAMWEB, 2014). Smoldering combustion is less efficient than flaming combustion, producing more CH_4 per unit mass of fuel consumed than flaming combustion, which would increase the $\Delta CH_4/\Delta CO_2$ ratio (Yokelson et al., 2008). This finding is in good agreement with the reported activity of the Rim wildfire shown in Fig. 2. The CH_4 ER's reported in this study are in good agreement with those reported by Urbanski (2013) from four wildfire-season fires in mixed conifer forests of the northern Rocky Mountains (USA), who reported CH_4 ER values of 7.4–22.0 ppb CH_4 (ppm CO_2)$^{-1}$.

3.4. Breif comparison with other studies

Emission factors, EF's, are typically calculated using the carbon mass balance approach (Yokelson et al., 1999) (see Equation (2)). The mass fraction of carbon in the fuel, F_c, is assumed to be 500 g kg^{-1} (reported to be accurate to 10% (Susott et al., 1996; Yokelson et al., 1999)); MM_x is the molar mass of species, x, (MM = 12 for carbon); and ΔC_i is the excess mass carbon in each species, which is calculated using ER's. The total carbon emitted from the fire is estimated using only ΔCO_2, ΔCO and ΔCH_4, resulting in an overestimation of EF by ~5% (Yokelson et al., 1999). EF's for the Rim wildfire were calculated from the SEAC^{4}RS flights on 26 and 27 August 2013 for a range of long-lived compounds (See Table 1).

$$EFx = F_c \times \frac{MM_x}{12} \times \frac{\Delta x}{\Delta C_{CO_2} + \Delta C_{CO} + \Delta C_{CH_4}} \quad (3)$$

Given that CO was not measured during AJAX flights, we use the SEAC^{4}RS data to calculate estimated emission factors. The similarity of ERs observed during the primary, intense burning period imply a similarity in fire conditions (see Fig. 9). Hence, we assume MCE to be the same on these days and use the median MCE calculated from SEAC^{4}RS flight data to calculate EFs for measured CO_2 and CH_4 during the AJAX flight on 29 August 2013. For 10 September 2013 we use MCE of 0.88, reported by Urbanski (2014) to estimate EFs for CO_2 and CH_4 (see Table 1). EFs and MCE calculated for the Rim wildfire compare well to previous studies as shown in Table 1. There are a wide number of variables which alter fire EFs including fire combustion stage, fuel type and condition, meteorological conditions and distance of sample from fire source. Table 1 highlights some of the variety of EFs measured over North America during different measurement campaigns, as well as the complexity in analyzing fire EFs. For example, CH_4 EFs from the Rim wildfire during the primary, intense burning period agree closely with previously reported values from Boreal wildfires (Simpson et al., 2011) and Rocky Mountain wildfires (Urbanski, 2013). During the increased smoldering, slower growth period of the Rim wildfire, CH_4 EFs are elevated but not to the same extent as the CH_4 EFs reported from Californian wildfires during ARCTAS-CA. In all cases, Rim wildfire CH_4 EFs are increased relative to those from prescribed fires reported by Burling et al. (2011).

4. Discussion and summary

Emissions from the Rim wildfire were sampled by two airborne

Table 1
MCE, ER and EF (±1-sigma uncertainty) of selected species relative to CO from the Rim wildfire compared to previous studies.

	Rim fire			ARCTAS-CA California biomass burning plumes[a]	ARCTAS Boreal forest fires	Rocky Mountains conifer forest fires	Temperate forest fires	Prescribed conifer forest understory fires
	26 Aug-13 intense	29-Aug-13 intense	10-Sep-13 smoldering		Simpson et al. (2011)	Urbanski (2013)[e]	Akagi et al. (2013)[f]	Burling et al. (2011)[f]
MCE EFCO	0.94[b] 92.5 ± 16	0.94[c] 69.5 ± 12	0.88[d] 138.4 ± 24	0.90,164.1 ± 28	0.89,113 ± 72	0.85–0.92 89.3–173	0.93 79 ± 19	0.94 72 ± 26
$EFCO_2$	1675 ± 285	1711 ± 292	1595 ± 272	1572 ± 268	1616 ± 180	1527 – 1681	1675 ± 42	1668 ± 72
$EFCH_4$	4.8 ± 0.8	4.7 ± 0.8	7.5 ± 1.3	13.0 ± 2.2	4.7 ± 2.9	4.4–12.1	2.7 ± 1.8	3.0 ± 2.4
$EFCH_3CN$	0.14 ± 0.03	–	–	0.31 ± 0.07	0.30 ± 0.06	–	0.03 ± -	–
EFC_3H_6O	0.56 ± 0.1	–	–	0.85 ± 0.2	0.37 ± 0.1	–	0.65 ± 0.3	–
$EFCH_3OH$	1.6 ± 0.4	–	–	1.9 ± 0.4	1.2 ± 0.3	–	1.2 ± 0.5	1.1 ± 1.0
EFC_6H_6	0.40 ± 0.07	–	–	0.63 ± 0.1	0.55 ± 0.11	–	0.28 ± 0.4	–
EF C_7H_8	0.26 ± 0.05	–	–	0.25 ± 0.04	0.24 ± 0.06	–	0.20 ± 0.3	–

[a] Data from Californian wildfires observed during ARCTAS-CA DC-8 study calculated based on archived data. (http://www-air.larc.nasa.gov/cgi-bin/ArcView/arctas).
[b] Median MCE from SEAC^{4}RS observations.
[c] MCE assumed to be the same as that observed during the SEAC^{4}RS flights on 26, 27 August 2013.
[d] MCE assumed to be 0.88, as reported for wildfires in northwest US conifer forests fires (Urbanski, 2014).
[e] Urbanski (2013) data shows range of values (minimum – maximum).
[f] Akagi et al. (2013) and Burling et al. (2011) data reported are average airborne EF's.

platforms during the fire's intense, primary burning period (flights on 26, 27 and 29 August 2013) and increased smoldering, slower growth period (flight on 10 September 2013). Trace gases showed considerable variability, with notable deviations from background levels observed within the SJV boundary layer and within the Rim wildfire smoke plume.

During the primary burning period, Lidar data shows the vertical extent and progression of the Rim wildfire plume. Emissions from the Rim wildfire were sampled by flights during the afternoon when Lidar data shows that the main, concentrated plume has started to dissipate and mix to higher elevations. During three flights (26, 27 and 29 August 2013), the main smoke plume was transported north/northeastwards. Airborne measurements show large deviations from background levels in many trace gas species when sampling emissions from the Rim wildfire.

The three flights during the primary burning period all support the concept of rapid O_3 formation resulting from the Rim wildfire, with ΔO_3 up to 100 ppb (26 August 2012) and 105 ppb (29 August 2013) observed within the upper layers of the smoke plume, within close proximity to the Rim wildfire source. The high ΔO_3 measured aloft were not observed at surface sites in downwind regions impacted by the plume. The AJAX flight observed much higher ΔO_3 in the main plume (aloft) than in a local smoke-filled valley, perhaps indicating that boundary layer measurements of ΔO_3 in smoke affected regions may be more applicable for determining impacts of wildfires on local regions than measurements from the main smoke plume, which can overshoot the boundary layer and be transported large distances as observed in the SEAC^{4}RS flights on 26/27 August 2013.

The AJAX flight on 10 September 2013 occurred during the Rim wildfire increased smoldering period. Meteorological conditions were markedly different to previous flights. The previous overnight down-slope easterly winds brought the Rim wildfire smoke plume into California's SJV, and daytime stagnant conditions on 10 September 2013 kept smoke impacts high in the region. ΔCO_2 values within the SJV boundary layer were similar in magnitude to those observed within the smoke plume, and ΔCH_4 values were much higher as a result of combined Rim wildfire smoke influence and local CH_4 emissions.

In the fresh smoke plume, there was a strong correlation between ΔCH_4 and ΔCO_2. Emission ratios were 8.0 ppb CH_4 (ppm CO_2)$^{-1}$ on 26 August, 6.5 ppb CH_4 (ppm CO_2)$^{-1}$ on 29 August, and 18.3 ppb CH_4 (ppm CO_2)$^{-1}$ on 10 September 2013. The increase in CH_4 ER from 6.5 to 8.0 ppb CH_4 (ppm CO_2)$^{-1}$ during the 26 and 29 August 2013 period to 18.3 ppb CH_4 (ppm CO_2)$^{-1}$ on 10 September 2013 likely indicates enhanced CH_4 emissions from increased smoldering combustion relative to flaming combustion on 10 September 2013 and a difference in fire fuel types. The wide range in CH_4 ER in fresh plumes from the Rim Fire on the different flight days represents the unique and variable nature of a wildfire plume during the fire's lifetime and progression.

Characterization of wildfire emissions is crucial for understanding atmospheric trace gas budgets and variability. The quality of these characterizations depends on accurate observations associated with fuel type, meteorological conditions and fire combustion burn cycle. Observations are key in validating forward model predictions of trace gas emissions (including greenhouse gases), transport, chemistry, and plume injection heights associated with the wildfires. This study provides a set of wildfire ERs and EFs taken close to the emission source of an extremely large wildfire during a prolonged drought. These observations coupled with wildfire emission inventories, estimates of fossil fuel emissions and background concentrations could be used to determine contributions of the Rim wildfire emissions to trace gas budgets by the use of inverse modeling.

Acknowledgments

We acknowledge the support and partnership of H211 L. L. C. for the Alpha Jet and the NASA Earth Science Program for the SEAC^{4}RS effort. Further support was provided by San Jose State University Research Foundation, the NASA Postdoctoral Program, the Bay Area Environmental Research Institute, the National Science Foundation (AGS-1151930) and the Ames Research Center. CH_3CN, CH_3OH, CH_3COCH_3, C_6H_6 and C_7H_8 measurements aboard the NASA DC-8 were supported by the Austrian Federal Ministry for Transport, Innovation and Technology (bmvit) through the Austrian Space Applications Programme (ASAP) of the Austrian Research Promotion Agency (FFG). AW and TM received support from the Visiting Scientist Program of the National Institute of Aerospace (NIA) and through NASA Earth Science Division Award NNX14AP4 We are thankful to the SEAC^{4}RS and Alpha Jet Science Teams for their contribution.

Appendix A. Supplementary data

Supplementary data related to this article can be found at http://dx.doi.org/10.1016/j.atmosenv.2015.12.038.

References

Airnow, 2015. http://www.airnow.gov/index.cfm?action=airnow.mapsarchivecalendar accessed 4 November 2015.

Akagi, S.K., Yokelson, R.J., Wiedinmyer, C., Alvarado, M.J., Reid, J.S., Karl, T., Crounse, J.D., Wennberg, P.O., 2011. Emission factors for open and domestic biomass burning for use in atmospheric models. Atmos. Chem. Phys. 11, 4039–4072.

Akagi, S.K., Craven, J.S., Taylor, J.W., McMeeking, G.R., Yokelson, R.J., Burling, I.R., Urbanski, S.P., Wold, C.E., Seinfeld, J.H., Coe, H., Alvarado, M.J., Weise, D.R., 2012. Evolution of trace gases and particles emitted by a chaparral fire in California. Atmos. Chem. Phys. 12, 1397–1421.

Akagi, S.K., Yokelson, R.J., Burling, I.R., Meinardi, S., Simpson, I., Blake, D.R., McMeeking, G.R., Sullivan, A., Lee, T., Kreidenweis, S., Urbanski, S., Reardon, J., Griffith, D.W.T., Johnson, T.J., Weise, D.R., 2013. Measurements of reactive trace gases and variable O_3 formation rates in some South Carolina biomass burning plumes. Atmos. Chem. Phys. 13, 1141–1165.

Andreae, M.O., Merlet, P., 2001. Emission of trace gases and aerosols from biomass burning. Glob. Biogeochem. Cy. 15, 955–966.

Aurell, J., Gullett, B.K., 2013. Emission factors from Aerial and ground measurements of field and laboratory Forest Burns in the Southeastern U.S.: PM2.5, black and brown carbon, VOC, and PCDD/PCDF. Environ. Sci. Technol. 47, 8443–8452.

Bein, K.J., Zhao, Y., Johnston, M.V., Wexler, A.S., 2008. Interactions between boreal wildfire and urban emissions. J. Geo. Phys. Res. 113. D07304.

Burling, I.R., Yokelson, R.J., Akagi, S.K., Urbanski, S.P., Wold, C.E., Griffith, D.W.T., Johnson, T.J., Reardon, J., Weise, D.R., 2011. Airborne and ground-based measurements of the trace gases and particles emitted by prescribed fires in the United States. Atmos. Chem. Phys. 11, 12197–12216.

Chen, H., Winderlich, J., Gerbig, C., Hoefer, A., Rella, C.W., Crosson, E.R., Van Pelt, A.D., Steinbach, J., Kolle, O., Beck, V., Daube, B.C., Gottlieb, E.W., Chow, V.Y., Santoni, G.W., Wofsy, S.C., 2010. High-accuracy continuous airborne measurements of greenhouse gases (CO2 and CH4) using the cavity ring-down spectroscopy (CRDS) technique. Atmos. Meas. Tech. 3, 375–386.

Clements, C.B., Oliphant, A., 2014. The California State University- Mobile Atmospheric Profiling System (CSU-MAPS): a facility for research and education in boundary-layer meteorology. Bull. Amer. Meteor. Soc. 95, 1713–1724.

Crutzen, P.J., Andreae, M.O., 1990. Biomass burning in the tropics: Impact on atmospheric chemistry and biogeochemical cycles. Science 250 (4988), 1669–1678.

Dale, L., 2006. Wildfire policy and fire use on public lands in the United States. Soc. Nat. Resour. 19, 275–284.

DeCarlo, P.F., Dunlea, E.J., Kimmel, J.R., Aiken, A.C., Sueper, D., Crounse, J., Wennberg, P.O., Emmons, L., Shinozuka, Y., Clarke, A., Zhou, J., Tomlinson, J., Collins, D.R., Knapp, D., Weinheimer, A.J., Montzka, D.D., Campos, T., Jimenez, J.L., 2008. Fast airborne aerosol size and chemistry measurements above Mexico City and Central Mexico during the MILAGRO campaign. Atmos. Chem. Phys. 8, 4027–4048. http://dx.doi.org/10.5194/acp-8-4027-2008.

Deeming, J.E., Burgan, R.E., Cohen, J.D., 1978. The 1978 National Fire-danger Rating System. Gen. Tech. Rep. INT-39. USDA Forest Service, Ogden, UT.

Dibb, J.E., Talbot, R.W., Scheuer, E., Seid, G., Avery, M.A., ingh, H.B., 2003. Aerosol chemical composition in Asian continental outflow during TRACE-P: Comparison to PEM-West B. J. Geophys. Res. 108 (D21) http://dx.doi.org/10.1029/2002JD003111, 8815.

Diskin, G.S., Podolske, J.R., Sachse, G.W., Slate, T.A., 2002. Open-path airborne

tunable 15 diode laser Hygrometer, in diode Lasers and applications in: atmospheric sensing. SPIE Proc. 4817, 196–204. http://dx.doi.org/10.1117/12.453736.
Evans, L.F., King, N.K., Packham, D.R., Stephens, E.T., 1974. Ozone measurements in smoke from forest fires. Environ. Sci. Techol 8 (1), 75–76.
FAMWEB, 2014. http://fam.nwcg.gov/fam-web/hist_209/hist_r_list_209s_2013?v_gaid=SO&v_209_number=CA-STF-002857&button= accessed 16 October 2014.
Forrister, H., Liu, J., Scheuer, E., Dibb, J., Ziemba, L., Thornhill, K.L., Anderson, B., Diskin, G., Perring, A.E., Schwarz, J.P., Campuzano-Jost, P., Day, D.A., Jimenez, J.L., Nenes, A., Weber, R.J., 2015. Evolution of brown carbon in wildfire plumes. Geophys. Res. Lett. 42, 4623–4630.
Fried, J., Torn, M., Mills, E., 2004. The impact of climate change on wildfire Severity: a regional Forecast for northern California. Clim. Chang. 64, 169–191.
Hecobian, A., Liu, Z., Hennigan, C.J., Huey, L.G., Jimenez, J.L., Cubison, M.J., Vay, S., Diskin, G.S., Sachse, G.W., Wisthaler, A., Mikoviny, T., Weinheimer, A.J., Liao, J., Knapp, D.J., Wennberg, P.O., Kürten, A., Crounse, J.D., Clair, J.S., Wang, Y., Weber, R.J., 2011. Comparison of chemical characteristics of 495 biomass burning plumes intercepted by the NASA DC-8 aircraft during the ARCTAS/CARB-2008 field campaign. Atmos. Chem. Phys. 11, 13325–13337.
Hobbs, P.V., Sinha, P., Yokelson, R.J., Christian, T.J., Blake, D.R., Gao, S., Kirchstetter, T.W., Novakov, T., Pilewskie, P., 2003. Evolution of gases and particles from a savanna fire in South Africa. J. Geophys. Res. 108 (D13), 8485.
Hornbrook, R.S., Blake, D.R., Diskin, G.S., Fried, A., Fuelberg, H.E., Meinardi, S., Mikoviny, T., Richter, D., Sachse, G.W., Vay, S.A., Walega, J., Weibring, P., Weinheimer, A.J., Wiedinmyer, C., Wisthaler, A., Hills, A., Riemer, D.D., Apel, E.C., 2011. Observations of nonmethane organic compounds during ARCTAS - Part 1: biomass burning emissions and plume enhancements. Atmos. Chem. Phys. 11, 11103–11130.
Huey, L.G., 2007. Measurement of trace atmospheric species by chemical ionization mass spectrometry: speciation of reactive nitogen and future directions. Mass Spectrom. Rev. 26, 166–184.
Hurteau, M.D., Westerling, A.L., Wiedinmyer, C., Bryant, B.P., 2014. Projected effects of climate and development on California wildfire emissions through 2100. Environ. Sci. Technol. 48, 2298–2304.
Jacob, D.J., Crawford, J.H., Maring, H., Clarke, A.D., Dibb, J.E., Emmons, L.K., Ferrare, R.A., Hostetler, C.A., Russell, P.B., Singh, H.B., Thompson, A.M., Shaw, G.E., McCauley, E., Pederson, J.R., Fisher, J.A., 2010. The Arctic Research of the Composition of the Troposphere from Aircraft and Satellites (ARCTAS) mission: design, execution, and first results. Atmos. Chem. Phys. 10, 5191–5212.
Jaffe, D.A., Wigder, N., Downey, N., Pfister, G., Boynard, A., Reid, S.B., 2013. Impact of wildfires on ozone exceptional events in the western U.S. Environ. Sci. Technol. 47, 11065–11072.
Jaffe, D.A., Wigder, N.L., 2012. Ozone production from wildfires: a critical review. Atmos. Environ. 51, 1–10.
Karion, A., Sweeney, C., Pétron, G., Frost, G., Michael Hardesty, R., Kofler, J., Miller, B.R., Newberger, T., Wolter, S., Banta, R., Brewer, A., Dlugokencky, E., Lang, P., Montzka, S.A., Schnell, R., Tans, P., Trainer, M., Zamora, R., Conley, S., 2013. Methane emissions estimate from airborne measurements over a western United States natural gas field. Geophys. Res. Lett. 40, 4393–4397.
Langenfelds, R.L., Francey, R.J., Pak, B.C., Steele, L.P., Lloyd, J., Trudinger, C.M., Allison, C.E., 2002. Interannual growth rate variations of atmospheric CO2 and its δ13C, H2, CH4, and CO between 1992 and 1999 linked to biomass burning. Glob. Biogeochem. Cy. 16, 1048.
Moteki, N., Kondo, Y., 2007. Effects of mixing state on black carbon measurements by laser-induced incandescence. Aerosol Sci. Technol. 41, 398–417.
NIFC, 2015. Geographic Area Coordination Center Statistics. http://www.predictiveservices.nifc.gov/intelligence/2011_statssumm/2011Stats&Summ.html. accessed 4 November 2015.
Packham, D.R., Vines, R.G., 1978. Properties of bushfire smoke: the reduction in visibility resulting from prescribed fires in forests. J. Air Pollut. Control Assoc. 28 (8), 790–795.
Peterson, D.A., Hyer, E.J., Campbell, J.R., Fromm, M.D., Hair, J.W., Butler, C.F., Fenn, M.A., 2014. The 2013 rim Fire: implications for predicting extreme fire spread, pyroconvection, and smoke emissions. Bull. Amer. Meteor. Soc. 96, 229–247.
Pfister, G.G., Wiedinmyer, C., Emmons, L.K., 2008. Impacts of the fall 2007 California wildfires on surface ozone: Integrating local observations with global model simulations. Geophys. Res. Lett. 35. L19814.
Real, E., Law, K.S., Weinzierl, B., Fiebig, M., Petzold, A., Wild, O., Methven, J., Arnold, S., Stohl, A., Huntrieser, H., Roiger, A., Schlager, H., Stewart, D., Avery, M., Sachse, G., Browell, E., Ferrare, R., Blake, D., 2007. Processes influencing ozone levels in Alaskan forest fire plumes during long-range transport over the North Atlantic. J. Geophys. Res. 112. D10S41.
Reid, J.S., Eck, T.F., Christopher, S.A., Koppmann, R., Dubovik, O., Eleuterio, D.P., Holben, B.N., Reid, E.A., Zhang, J., 2005. A review of biomass burning emissions part III: intensive optical properties of biomass burning particles. Atmos. Chem. Phys. 5, 827–849.
Sachse, G.W., Hill, G.F., Wade, L.O., Perry, M.G., 1987. Fast-resposnse, high-precision carbon monoxide sensor using a tunable diode laser absorption technique. J. Geophys. Res. 92 (D2), 2071–2081.
Saide, P.E., Peterson, D., da Silva, A., Anderson, B., Ziemba, L.D., Diskin, G., Sachse, G., Hair, J., Butler, C., Fenn, M., Jimenez, J.L., Campuzano-Jost, P., Perring, A., Schwarz, J., Markovic, M.Z., Russell, P., Redemann, J., Shinozuka, Y., Streets, D.G., Yan, F., Dibb, J., Yokelson, R., Toon, O.B., Hyer, E., Carmichael, G.R., 2015. Revealing important nocturnal and day-to-day variations in fire smoke emissions through a novel multiplatform inversion. Geophys. Res. Lett. 42, 3609–3618.
Sapkota, A., Symons, J.M., Kleissl, J., Wang, L., Parlange, M.B., Ondov, J., Breysse, P.N., Diette, G.B., Eggleston, P.A., Buckley, T.J., 2005. Impact of the 2002 Canadian Forest fires on particulate matter air quality in Baltimore City. Environ. Sci. Technol. 39, 24–32.
Simpson, I.J., Akagi, S.K., Barletta, B., Blake, N.J., Choi, Y., Diskin, G.S., Fried, A., Fuelberg, H.E., Meinardi, S., Rowland, F.S., Vay, S.A., Weinheimer, A.J., Wennberg, P.O., Wiebring, P., Wisthaler, A., Yang, M., Yokelson, R.J., Blake, D.R., 2011. Boreal forest fire emissions in fresh Canadian smoke plumes: C1-C10 volatile organic compounds (VOCs), CO2, CO, NO2, NO, HCN and CH3CN. Atmos. Chem. Phys. 11, 6445–6463.
Simpson, I.J., Rowland, F.S., Meinardi, S., Blake, D.R., 2006. Influence of biomass burning during recent fluctuations in the slow growth of global tropospheric methane. Geophys.l Res. Lett. 33. L22808.
Singh, H.B., Anderson, B.E., Brune, W.H., Cai, C., Cohen, R.C., Crawford, J.H., Cubison, M.J., Czech, E.P., Emmons, L., Fuelberg, H.E., Huey, G., Jacob, D.J., Jimenez, J.L., Kaduwela, A., Kondo, Y., Mao, J., Olson, J.R., Sachse, G.W., Vay, S.A., Weinheimer, A., Wennberg, P.O., Wisthaler, A., 2010. Pollution influences on atmospheric composition and chemistry at high northern latitudes: boreal and California forest fire emissions. Atmos. Environ. 44, 4553–4564.
Singh, H.B., Cai, C., Kaduwela, A., Weinheimer, A., Wisthaler, A., 2012. Interactions of fire emissions and urban pollution over California: ozone formation and air quality simulations. Atmos. Environ. 56, 45–51.
Susott, R.A., Olbu, G.J., Baker, S.P., Ward, D.E., Kauffman, J.B., Shea, R.W., 1996. Carbon, hydrogen, nitrogen and thermogravimetric analysis of tropical ecosystem biomass. In: Biomass Burning and Global Change. MIT Press, Cambridge, MA, pp. 350–360.
Tadić, J.M., Loewenstein, M., Frankenberg, C., Butz, A., Roby, M., Iraci, L.T., Yates, E.L., Gore, W., Kuze, A., 2014. A comparison of in situ aircraft measurements of carbon dioxide and methane to GOSAT data measured over Railroad Valley playa, Nevada, USA. IEEE Trans. Geosci. Remote Sens. 52, 7764–7774.
Tanaka, T., Miyamoto, Y., Morino, I., Machida, T., Nagahama, T., Sawa, Y., Matsueda, H., Wunch, D., Kawakami, S., Uchino, O., 2012. Aircraft measurements of carbon dioxide and methane for the calibration of ground-based high-resolution Fourier Transform Spectrometers and a comparison to GOSAT data measured over Tsukuba and Moshiri. Atmos. Meas. Tech. 5, 2003–2012.
Toon, O.B., et al., 2015. Planning, implementation and scientific goals of the studies of emissions and atmospheric composition, clouds and climate coupling by regional surveys (SEAC^{4}RS) field mission. J. Geophys. Res. (In Preparation).
Trentmann, J., Andreae, M.O., Graf, H.-F., 2003. Chemical processes in a young biomass-burning plume. J. Geophys. Res. 108 (D22), 4705.
Urbanski, S.P., 2013. Combustion efficiency and emission factors for wildfire-season fires in mixed conifer forests of the northern Rocky Mountains, US. Atmos. Chem. Phys. 13, 7241–7262.
Urbanski, S., 2014. Wildland fire emissions, carbon, and climate: emission factors. For. Ecol. Manage. 317, 51–60.
van der Werf, G.R., Randerson, J.T., Giglio, L., Collatz, G.J., Mu, M., Kasibhatla, P.S., Morton, D.C., DeFries, R.S., Jin, Y., van Leeuwen, T.T., 2010. Global fire emissions and the contribution of deforestation, savanna, forest, agricultural, and peat fires (1997–2009). Atmos. Chem. Phys. 10, 11707–11735.
Vay, S.A., Woo, J.-H., Anderson, B.E., Thornhill, K.L., Blake, D.R., Westberg, D.J., Kiley, C.M., Avery, M.A., Sachse, G.W., Streets, D., Tsutsumi, Y., Nolf, S., 2003. The influence of regional-scale anthropogenic emissions on CO_2 distributions over the western North Pacific. J. Geophys. Res. 108, 8801.
Westerling, A.L., Hidalgo, H.G., Cayan, D.R., Swetnam, T.W., 2006. Warming and Earlier Spring increase western U.S. Forest wildfire activity. Science 313, 940–943.
Wigder, N.L., Jaffe, D.A., Saketa, F.A., 2013. Ozone and particulate matter enhancements from regional wildfires observed at Mount Bachelor during 2004–2011. Atmos. Environ. 75, 24–31.
Weinheimer, A.J., Walega, J.G., Ridley, B.A., Gary, B.L., Blake, D.R., Blake, N.J., Rowland, F.S., Sachse, G.W., Anderson, B.E., Collins, J.E., 1994. Meridional distributions of NOx, NOy, and other species in the lower stratosphere and upper troposphere during AASE II. Geophys. Res. Lett. 21, 2583–2586.
Wisthaler, A., Hansel, A., Dickerson, R.R., Crutzen, P.J., 2002. Organic trace gas measurements by PTR-MS during INDOEX 1999. J. Geophys. Res. 107, 8024.
Yokelson, R.J., Goode, J.G., Ward, D.E., Susott, R.A., Babbitt, R.E., Wade, D.D., Bertschi, I., Griffith, D.W.T., Hao, W.M., 1999. Emissions of formaldehyde, acetic acid, methanol, and other trace gases from biomass fires in North Carolina measured by airborne Fourier transform infrared spectroscopy. J. Geophys. Res. 104, 30109–30125.
Yokelson, R.J., Christian, T.J., Karl, T.G., Guenther, A., 2008. The tropical forest and fire emissions experiment: laboratory fire measurements and synthesis of campaign data. Atmos. Chem. Phys. 8, 3509–3527.
Yokelson, R.J., Andreae, M.O., Akagi, S.K., 2013. Pitfalls with the use of enhancement ratios or normalized excess mixing ratios measured in plumes to characterize pollution sources and aging. Atmos. Meas. Tech. 6, 2155–2158.
Yue, X., Mickley, L.J., Logan, J.A., Kaplan, J.O., 2013. Ensemble projections of wildfire activity and carbonaceous aerosol concentrations over the western United States in the mid-21st century. Atmos. Environ. 77, 767–780.